Technical Report DEVCOMAC-BLTR-21008

Measurement of Corrosion Potential Under Thin Electrolyte Films and the Expression of Localized Corrosion Damage

Digby D. Macdonald[1]
George R. Engelhardt[2]
Jennifer A. Cordes[3]
Robert E. Dillon[4]
Daniel P. Schmidt[3]
Gregory N. Vigilante[4]
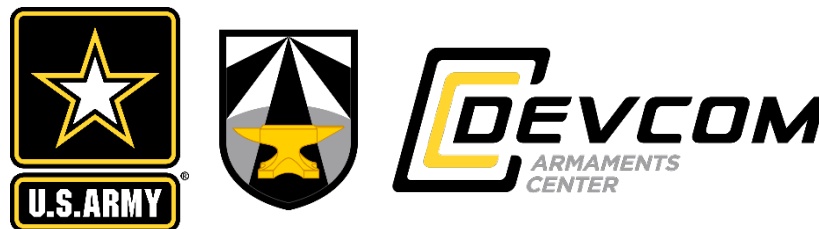Edward J. Troiano[4]
John J. Cannon[4]
Andrew G. Littlefield[4]

[1]Department of Nuclear Engineering
University of California at Berkeley
Berkeley, CA 94720, USA

[2]OLI Systems, Inc
Cedar Knowls, NJ 07927, USA

[3]U.S. Army Combat Capabilities
Development Command Armaments Center
Munitions Engineering and Technology Center
Picatinny Arsenal, NJ 07806-5000, USA

[4]U.S. Army Combat Capabilities
Development Command Armaments Center
Weapons and Software Engineering Center
Benét Laboratories
Watervliet, NY 12189

September 2019

REPORT DOCUMENTATION PAGE

1. REPORT DATE *(DD-MM-YYYY)*	2. REPORT TYPE	3. DATES COVERED *(From - To)*
09/01/2019		

4. TITLE AND SUBTITLE	5a. CONTRACT NUMBER
Measurement of Corrosion Potential Under Thin Electrolyte Films and the Expression of Localized Corrosion Damage	
	5b. GRANT NUMBER
	5c. PROGRAM ELEMENT NUMBER

6. AUTHOR(S)	5d. PROJECT NUMBER
Digby D. Macdonald, George R. Engelhardt, Jennifer A. Cordes, Robert E. Dillon, Daniel P. Schmidt, Gregory N. Vigilante, Edward Troiano, John J. Cannon, Andrew G. Littlefield	
	5e. TASK NUMBER
	5f. WORK UNIT NUMBER

7. PERFORMING ORGANIZATION NAME(S) AND ADDRESS(ES)	8. PERFORMING ORGANIZATION REPORT NUMBER
U.S. Army Combat Capabilities Development Command, Armaments Center Weapons and Software Engineering Center, Benét Laboratories Directorate 1 Buffington Street Watervliet, NY 12189	DEVCOMAC-BLTR-21008

9. SPONSORING/MONITORING AGENCY NAME(S) AND ADDRESS(ES)	10. SPONSOR/MONITOR'S ACRONYM(S)
	11. SPONSOR/MONITOR'S REPORT NUMBER(S)

12. DISTRIBUTION/AVAILABILITY STATEMENT
Distribution Statement A. Approved for public release

14. ABSTRACT
An analysis of cracking in vent holes in high-strength steel tubes is reported, with the predictions being judged to be highly conservative. Pitting and subsequent cracking is attributed to localized corrosion beneath a layer residue on the hole surface that accumulates with use. The residue contains a high concentration of chloride ion, which is well-known to be a powerful agent in affecting passivity breakdown and pitting on high strength steels, like AISI 4335. The measured corrosion potential at three locations on a AISI 4335 sample in contact with a thin slurry of residue under prototypical field conditions was found to be -0.255 ± 0.021 Vshe. Because this value is close to the breakdown potential (which was not measured und

15. SUBJECT TERMS
Pitting corrosion, stress corrosion cracking, corrosion fatigue, AISI 4340 steel, damage function analysis, Pareto distribution, failure

16. SECURITY CLASSIFICATION OF:			17. LIMITATION OF ABSTRACT	18. NUMBER OF PAGES	19a. NAME OF RESPONSIBLE PERSON
a. REPORT	b. ABSTRACT	c. THIS PAGE			Gregory N. Vigilante
					19b. TELEPHONE NUMBER *(Include area code)*
U/L	SAR	SAR	SAR	31	518-266-5204

INSTRUCTIONS FOR COMPLETING SF 298

1. REPORT DATE. Full publication date, including day, month, if available. Must cite at least the year and be Year 2000 compliant, e.g. 30-06-1998; xx-06-1998; xx-xx-1998.

2. REPORT TYPE. State the type of report, such as final, technical, interim, memorandum, master's thesis, progress, quarterly, research, special, group study, etc.

3. DATE COVERED. Indicate the time during which the work was performed and the report was written, e.g., Jun 1997 - Jun 1998; 1-10 Jun 1996; May - Nov 1998; Nov 1998.

4. TITLE. Enter title and subtitle with volume number and part number, if applicable. On classified documents, enter the title classification in parentheses.

5a. CONTRACT NUMBER. Enter all contract numbers as they appear in the report, e.g. F33315-86-C-5169.

5b. GRANT NUMBER. Enter all grant numbers as they appear in the report. e.g. AFOSR-82-1234.

5c. PROGRAM ELEMENT NUMBER. Enter all program element numbers as they appear in the report, e.g. 61101A.

5e. TASK NUMBER. Enter all task numbers as they appear in the report, e.g. 05; RF0330201; T4112.

5f. WORK UNIT NUMBER. Enter all work unit numbers as they appear in the report, e.g. 001; AFAPL30480105.

6. AUTHOR(S). Enter name(s) of person(s) responsible for writing the report, performing the research, or credited with the content of the report. The form of entry is the last name, first name, middle initial, and additional qualifiers separated by commas, e.g. Smith, Richard, J, Jr.

7. PERFORMING ORGANIZATION NAME(S) AND ADDRESS(ES). Self-explanatory.

8. PERFORMING ORGANIZATION REPORT NUMBER. Enter all unique alphanumeric report numbers assigned by the performing organization, e.g. BRL-1234; AFWL-TR-85-4017-Vol-21-PT-2.

9. SPONSORING/MONITORING AGENCY NAME(S) AND ADDRESS(ES). Enter the name and address of the organization(s) financially responsible for and monitoring the work.

10. SPONSOR/MONITOR'S ACRONYM(S). Enter, if available, e.g. BRL, ARDEC, NADC.

11. SPONSOR/MONITOR'S REPORT NUMBER(S). Enter report number as assigned by the sponsoring/ monitoring agency, if available, e.g. BRL-TR-829; -215.

12. DISTRIBUTION/AVAILABILITY STATEMENT. Use agency-mandated availability statements to indicate the public availability or distribution limitations of the report. If additional limitations/ restrictions or special markings are indicated, follow agency authorization procedures, e.g. RD/FRD, PROPIN, ITAR, etc. Include copyright information.

13. SUPPLEMENTARY NOTES. Enter information not included elsewhere such as: prepared in cooperation with; translation of; report supersedes; old edition number, etc.

14. ABSTRACT. A brief (approximately 200 words) factual summary of the most significant information.

15. SUBJECT TERMS. Key words or phrases identifying major concepts in the report.

16. SECURITY CLASSIFICATION. Enter security classification in accordance with security classification regulations, e.g. U, C, S, etc. If this form contains classified information, stamp classification level on the top and bottom of this page.

17. LIMITATION OF ABSTRACT. This block must be completed to assign a distribution limitation to the abstract. Enter UU (Unclassified Unlimited) or SAR (Same as Report). An entry in this block is necessary if the abstract is to be limited.

ABSTRACT

An analysis of cracking in vent holes in high-strength steel tubes is reported, with the predictions being judged to be highly conservative. Pitting and subsequent cracking is attributed to localized corrosion beneath a layer residue on the hole surface that accumulates with use. The residue contains a high concentration of chloride ion, which is well-known to be a powerful agent in affecting passivity breakdown and pitting on high strength steels, like AISI 4335. The measured corrosion potential at three locations on a AISI 4335 sample in contact with a thin slurry of residue under prototypical field conditions was found to be -0.255 ± 0.021 V_{she}. Because this value is close to the breakdown potential (which was not measured under exactly the same conditions) the electrochemical conditions are therefore judged to be conducive to passivity breakdown and hence pitting corrosion. The stress state of the region as determined by finite element analysis, is also judged to be conducive to the nucleation of cracks from pits. Using Damage Function Analysis (DFA) and a Pareto distribution for crack growth rate, the study successfully accounts for the evolution of localized corrosion damage and provides an effective means of extrapolating damage to future times, if the environmental conditions remain constant. The impact of stress transients during service on the accumulation of the observed damage (crack length) is judged to be negligible.

Table of Contents

List of Figures

List of Tables

1. Introduction

The US Army is currently experiencing localized corrosion damage to low alloy steels. The damage is manifest as pitting and cracking, where the cracks nucleate at pits.

Typical micrographs of the steel are shown in Figures 1. As revealed in Figure 1 (a), the microstructure is consistent with the tempered martensitic structure of this class of steel (AISI 4335), with the presence of inclusions [Figure 1(b)], probably MnS and/or carbides, with a relatively low density of 772 cm^{-2} (longitudinal) and 3603 cm^{-2} (transverse). This indicates that the material is a relatively "clean steel".
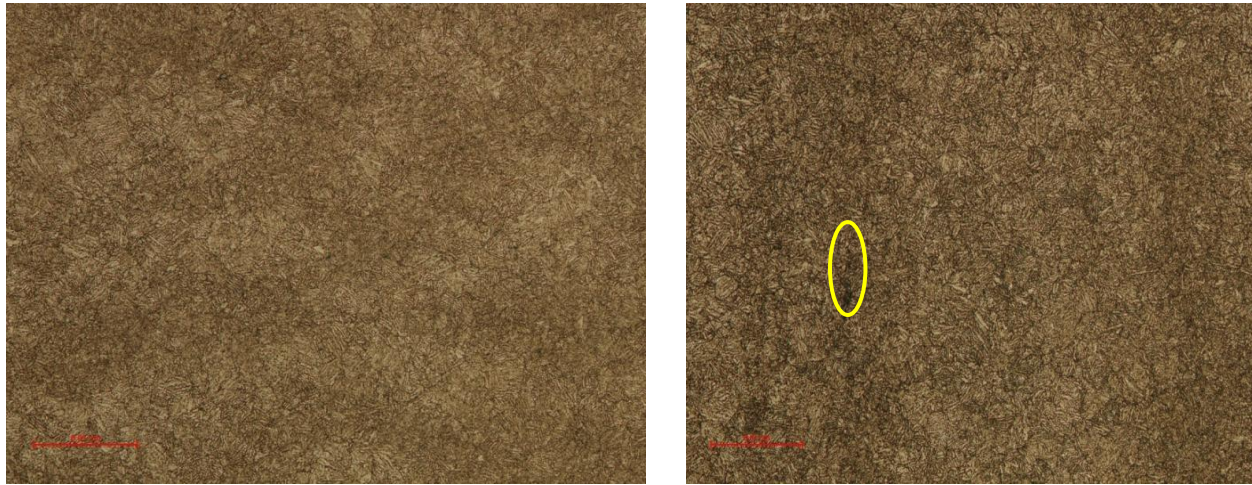
Figure 1: (a) Microstructure of the steel as viewed in the longitudinal direction. (b) Typical MnS or carbide inclusion highlighted in the micrograph.
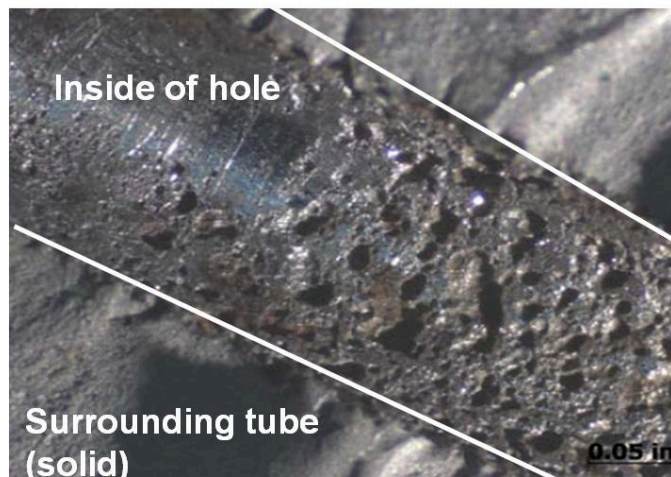
Figure 2: Photograph of the inside of the hole illustrating the deposited residue and corrosion.

The damage is found to occur in holes, an example of which is shown in Figure 2. The residue deposits on the surfaces of the hole is hydroscopic, by virtue of containing a significant amount of salts (e.g., NaCl, NaF, NaBr) that readily hydrate when in contact with moist air (Figure 2). This process results in the formation of a thin electrolyte film on the steel surface, which is a necessary condition for the development of the general and localized corrosion damage that is observed in the evacuator hole.

The objective of this research was to assess the probability that the current population of tubes may not suffer catastrophic failure within a specified time (500 cycles) and to formulate recommendations for extending the tube threshold life-time to 28 years. We also provide an estimate of our confidence level in extending the limit of condemned tubes to the end of the threshold period, assuming a maximum flaw allowable of 2.69 mm in a population of 226. These issues were addressed through a targeted experimental program at DEVCOM AC and in the author's (DDM's) laboratory, in support of a Damage Function Analysis [1-6] evaluation of the probability of failure.

1.1. Mechanical Properties

Some relevant physical, mechanical, and electrochemical properties of the steel are summarized in Table 1. These data will be used as input for estimating the crack growth rate using the Coupled Environment Fracture Model (CEFM) [7-20] in a subsequent paper. The CEFM has been used successfully to predict crack growth rate (CGR) in sensitized Type 304 SS, mill-annealed Alloys 600 and 690, AA 5083, and ASTM A470/471 turbine disk/rotor steels. The basis of the CEFM is that strong coupling exists between the crack internal environment and the external surfaces, upon which the cathodic reaction (oxygen reduction or hydrogen evolution) occurs, as envisioned in the differential aeration hypothesis (DAH) for localized corrosion. DAH is the generally accepted theoretical basis for the development of all forms of localized corrosion, except for hydrogen embrittlement. The governing condition is the conservation of charge, which enables specification of the electrostatic potential in the solution at the crack mouth. Once this potential is known, the coupled mass transfer (Nernst-Planck) and electrostatic equations (e.g., Laplace's or Poisson's equation) may be solved for both the cavity and the external environment to yield the coupling current and the crack growth rate (CGR) may be calculated using Faraday's law.

Table 1: Preliminary values for physical, mechanical, and electrochemical parameters in the CEFM for AISI 4335 high-strength, low alloy steel.

Parameter	Value.
Atomic volume (m^3)	1.18×10^{-29}
Fracture strain of oxide film, ε_f	8×10^{-4}
Young's modulus, E(MPa)	2.011e5
Dimensionless constant, β	5.08
Density, ρ(g/cm^3)	7.87
Yield strength, σ_y(MPa)	1093.3
Strain hardening exponent, n	1.7
Dimensionless constant, λ	0.11
Shear modulus, G(MPa)	7.855e4
Grain-boundary self-diffusion coefficient, D_{b0}(m^2/s)	7.24e-14 at 703 K.
Activation energy for diffusion (kJ/mol)	55.7
Grain-boundary diffusion width (m)	5×10^{-10}
Tafel slope for HER	0.065
i_0 for HER (A/cm^2)	5×10^{-4}
Tafel slope for ORR	0.071
i_0 for ORR (A/cm^2)	5.05×10^{-3}
Passive current density at steady state (A/cm^2)	2.6×10^{-3}
Standard electrochemical potential for stainless steel dissolution reaction, E_0(V$_{SHE}$)	-0.47

The CEFM is highly developed and has been applied to a variety of systems, as indicated above. While not included in the original statement of work, the CEFM, once calibrated on the crack growth rate data being measured at DEVCOM AC, the CEFM will allow us to predict CGR over a much greater range of conditions (temperature, potential, stress intensity factor, conductivity, etc.) than can be obtained by direct measurement, given the limited resources that are available. Currently, as noted above, CGR data are being measured at DEVCOM AC. These data will be used to calibrate the CEFM in a later phase of this program. Table 1 also contains important electrochemical kinetic data for the Hydrogen Evolution Reaction (HER) and the Oxygen Reduction Reaction (ORR), which occur on the external surfaces and annihilate the electron current emanating from the crack tip (or, equivalently, the ionic current flowing through the solution from the crack tip to the external surface). These data are important, because stress corrosion cracking (SCC) is predicted and found experimentally to be partly mechanical and partly electrochemical in character and any successful model must accurately reflect this duality of character. This important fact has been ignored in the development of other models for stress corrosion cracking, which tend to be purely mechanical in nature, with any electrochemistry being incorporated only inadvertently through calibration.
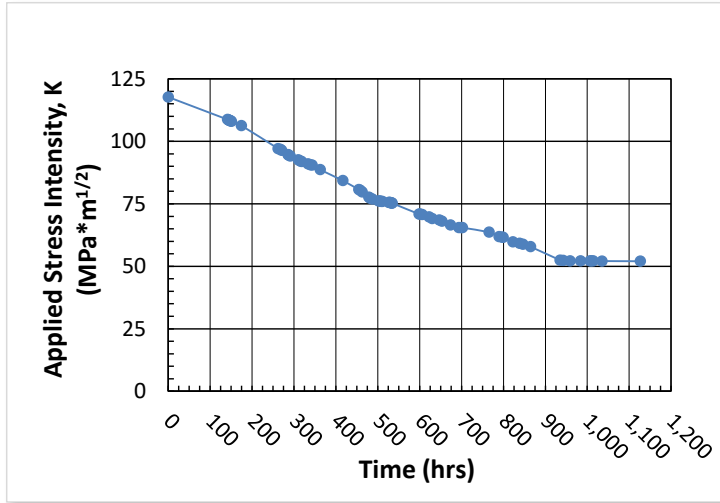
Figure 3: Variation of stress intensity with time for crack propagation through AISI 4335 steel in contact with residue under controlled humidity as measured using an instrumented bolt-loaded compact tension (CT) specimen. RH = 95 %, T = 104 °F (40 °C).

The crack growth rate data for AISI 4335 steel shown in Figure 3 were obtained at DEVCOM AC using an instrumented bolt-loaded, compact toughness (CT) specimen containing, initially, a fatigue crack, and loaded to an initial stress intensity factor of 120 MPa.m$^{1/2}$. The crack then propagated through the specimen under constant crack opening displacement conditions, resulting in a relaxation of the load and hence a decrease in the stress intensity factor, as shown in Figure 3. Crack arrest occurs when $K_I = K_{ISCC}$, yielding $K_{ISCC} = 51$ MPa.m$^{1/2}$. Note that the sides of the CT specimen were in contact with residue and the experiment was carried out in an environmental chamber at RH = 95 % at 104 °F. This experimental arrangement is recommended by ASTM (ASTM E1681-03, 2008) as the appropriate method for determining K_{ISCC}.
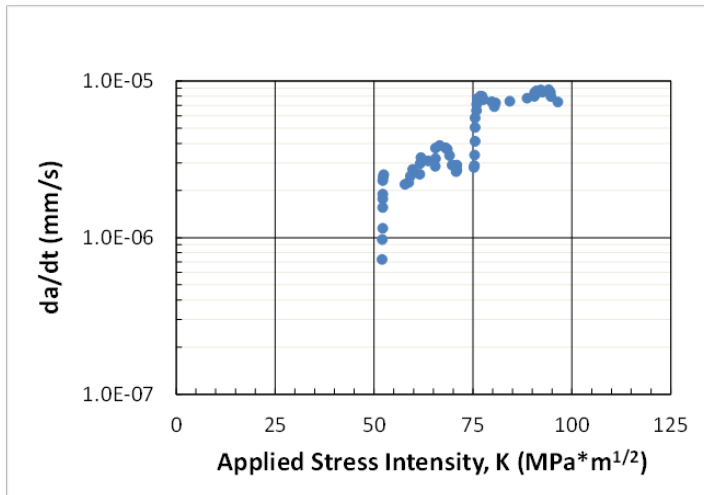
Figure 4: Variation of crack growth rate with stress intensity for crack propagation through AISI 4335 steel in contact with residue under controlled humidity as measured using a compact tension (CT) specimen under constant loading conditions. RH = 95 %, T = 104 °F (40 °C).

Figure 4 shows crack growth rate versus stress intensity factor data for crack propagation in AISI 4335 in contact with the residue, as determined by DEVCOM AC from the experiment outlined above. The reader will note that once $K_I > K_{ISCC} (= 51$ MPa.m$^{1/2}$), the crack growth rate increases sharply with increasing stress intensity and reaches a plateau value of ca. 9x10^{-6} mm/s. This is an exceptionally high crack growth rate, which may be

compared, for example with that observed (10^{-8} – 10^{-7} mm/s) in the closely-related low pressure steam turbine disk/rotor steel (ASTM A470/471) in contact with early condensate (an electrolyte phase that precipitates from steam at the exit of a low-pressure steam turbine). While a detailed analysis of crack growth rate is beyond the scope of the present project, we will attempt to identify the factors that cause this difference in a subsequent phase of the program. Significant "structure" is observed in the CGR vs K_I data, suggesting that the cracking was an intermittent process and that the cracking mechanism may involve hydrogen-induced cracking (HIC). Given the high strength/high hardness nature of this steel, this postulate is reasonable, but will need to be tested experimentally.

2. Experimental.

One of the key parameters in predicting the evolution of localized corrosion damage is the corrosion potential, which is the potential that a metal spontaneously adopts, as measured against a reference electrode, in a specified environment under open circuit conditions. In the clear majority of such measurements, the corrosion potential of a metal is measured in contact with a bulk electrolyte environment (e.g., bulk seawater), but in the case of the holes, the steel is in contact with a thin electrolyte surface film that forms by hydration of the residue. The presence of a thin electrolyte film greatly enhances the mass transport of oxygen to the metal surface with the result that the corrosion potential is displaced in the positive direction when compared with that measured in a bulk electrolyte environment. Accordingly, to ensure that the laboratory measurements of the corrosion potential accurately conform to the actual system, under the direction of the authors, the corrosion potential of the steel in contact with the residue was measured using the experimental arrangement shown in Figure 5.
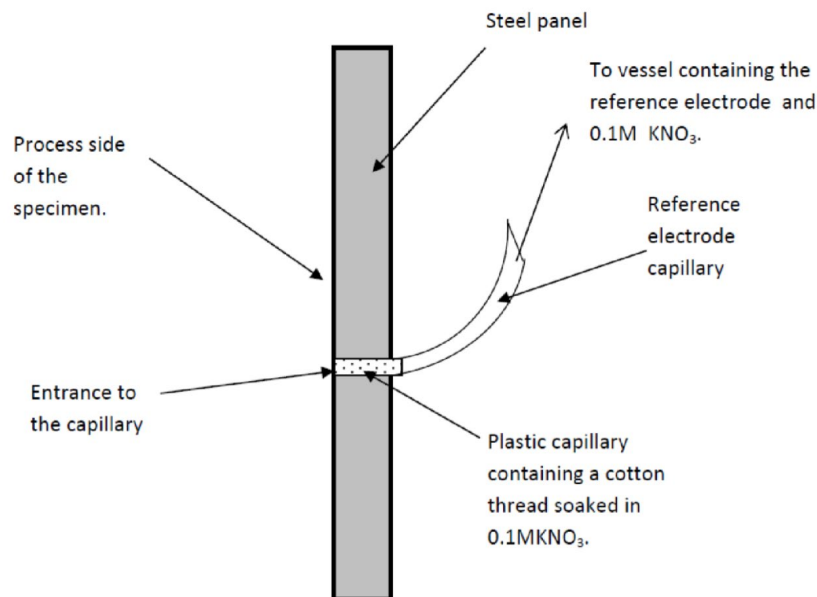
Figure 5: Reference electrode employed at DEVCOM AC for measuring the corrosion potential of AISI 4335 steel in contact with residue on the process side of the specimen.

The measured corrosion potential at three locations was found to be -0.520 V_{sce}, -0.480 V_{sce}, and 0.-0.496 V_{sce} at Holes 2, 5, and 8, respectively, in Panel 1A, corresponding to -0.276 V_{she}, -0.236 V_{she}, and -0.252 V_{she}, respectively, or an average of -0.255 ± 0.021 V_{she}. These values are eminently reasonable for the prevailing conditions [T = 75 °F (24 °C), pH = 10] and are used later in this paper for refining the calculation of pit nucleation rate and pit growth rate. Most importantly, this value will be used to assess the ability of the Mixed Potential Model (MPM) to predict the corrosion potential of the steel as the system transitions along the corrosion evolutionary path (CEP).

3. Results and Discussion

3.1. Expression of Localized Corrosion Damage

The experimental program underway that seeks to characterize the pitting damage functions for AISI 4335 steel exposed to residue for different exposure times. The data obtained from these laboratory studies are summarized in Figure 6. These damage functions are characterized by long tails at higher depths; a feature that is discussed below in terms of a Pareto distribution. Of particular importance is the observation that the maximum depth does not appear to be strongly-dependent upon time, suggesting that the deepest pits passivate (die) shortly after initial exposure.
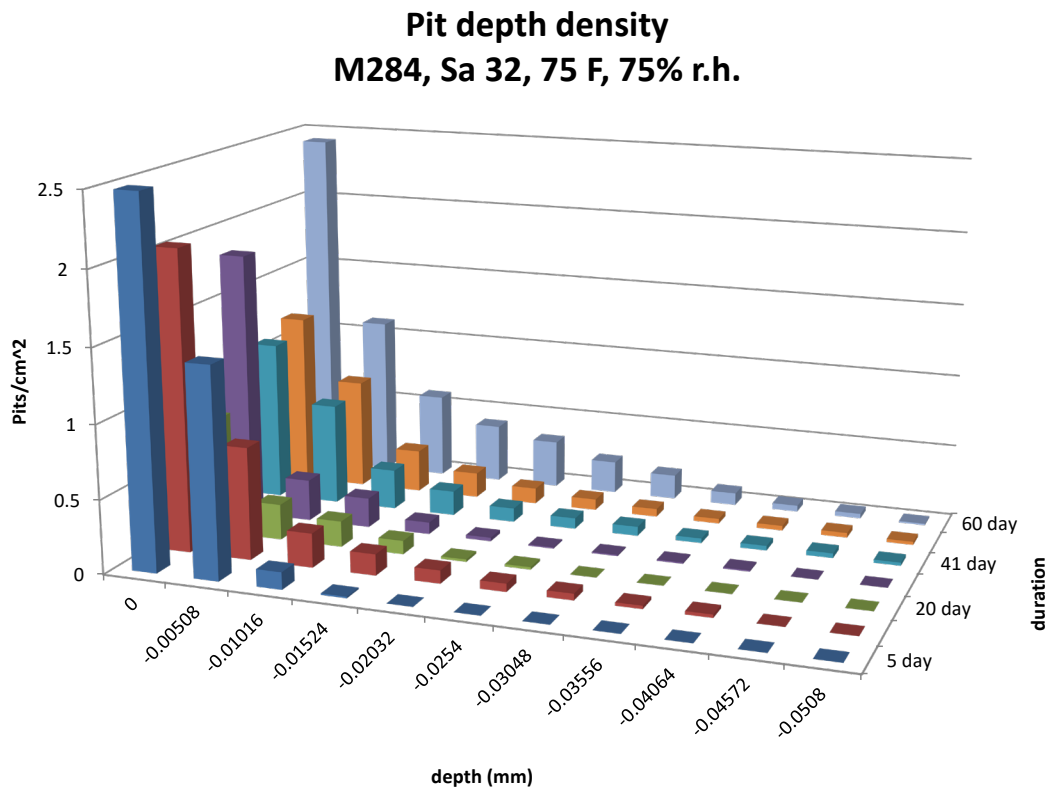
Figure 6: Integral damage functions for AISI 4335 in contact with residue after exposure for 5, 11, 20, 33, 41, 50, and 60 days in an environmental chamber at 75 °F (24 °C) and 75 % RH.

The damage function for each time displayed in Figure 6 were determined upon a separate sample and hence the observed damage is strictly not "cumulative" in nature. This is, because determination of the differential damage function (DDF) requires removal of the specimen and cleansing of the surface, which kills the pits. Since the pits are simply not reactivated by re-exposure to the environment, it is not possible to obtain the DDFs for all times from a single sample, at least not until some *in situ* method having the required resolution is developed for determining pit depth. Thus, because of the enormous complexity of localized corrosion, and since it is virtually impossible to control all the parameters that determine the rate of accumulation of damage, the DDFs do not always vary progressively with increasing observation time and the DDFs shown in Figure 6 are no exception. Nevertheless, much useful information can be gleaned from the data, as described below.
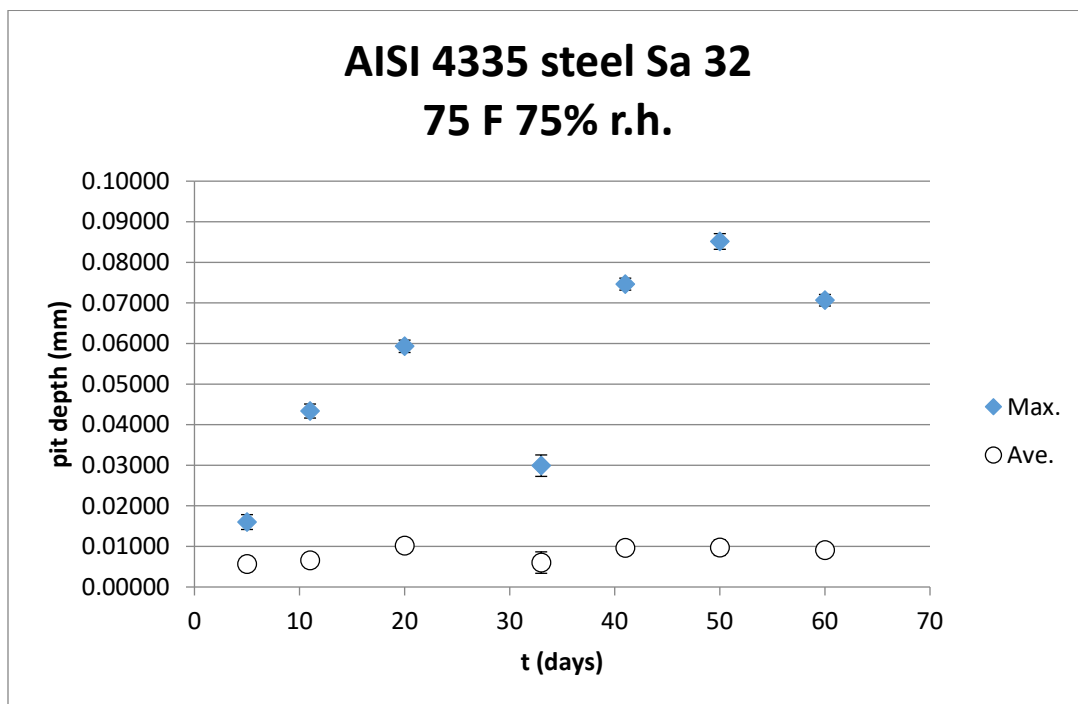
Figure 7: Evolution of the maximum and average pit depths for AISI 4335 steel in contact with residue at 75 °F and 75 % RH.

From Figure 7, it is evident that neither the maximum pit depth nor the average pit depth increases systematically and significantly with time, although the maximum appears to pass through a maximum. However, this is an artifact, because the maximum pit depth must increase with time or remain constant (in the case that the deepest pits are dead). Indeed, the data show that as time goes by, the maximum pit depth does trend to a constant value. However, the average pit depth remains invariant with time. This is characteristic of a system in which the pits are becoming progressively repassivated (are dying) as the observation time increases, such that few of the deepest pits are still active but that the average depth is dominated by the more numerous, shallow pits that have already passivated. This further indicates that the delayed repassivation constant, γ, is large, which is a desired condition for limiting the accumulation of localized corrosion damage.

There exist basically three mechanisms for pit repassivation (death) [1]: (1) **Death by Old Age**, in which the pit dies because the external surfaces can no longer provide the necessary resources, in terms of the oxygen reduction reaction (ORR), to maintain differential aeration. Differential aeration (DA), causes a positive, ionic current to flow through the solution from the pit mouth to the external surface where it annihilates with the electron current flowing through the metal from the pit cavity to the external surfaces, as depicted in Figure 8. The area on the external surface where annihilation occurs is defined by the "hemisphere of influence" (HOI), which is centered (ideally) upon the pit axis. The radius of the HOI is predicted to increase with the square root of pit age, but it cannot increase *ad infinitum* to supply ever increasing resources to support continued pit growth, because of the increasing IR potential drop through the external solution to the periphery of the HOI. Thus, at some critical distance from the pit axis insufficient potential drop will exist across the external/solution interface to drive the ORR. That defines the limit of the resources that are available to the pit from the external surface. As the pit continues to grow in size past that point, insufficient coupling current is available to maintain differential aeration and DA is lost. Once differential aeration is lost, the aggressive conditions that existed in the fit cavity (high $[H^+]$ and $[Cl^-]$), which maintained the pit cavity surfaces in the depassivated state, disperse by diffusion and the pit cavity surfaces passivate. This causes the pit to die. (2) **Death by Conflict.** In this scenario, neighboring pits compete for the available resources, such that only the fittest survives.
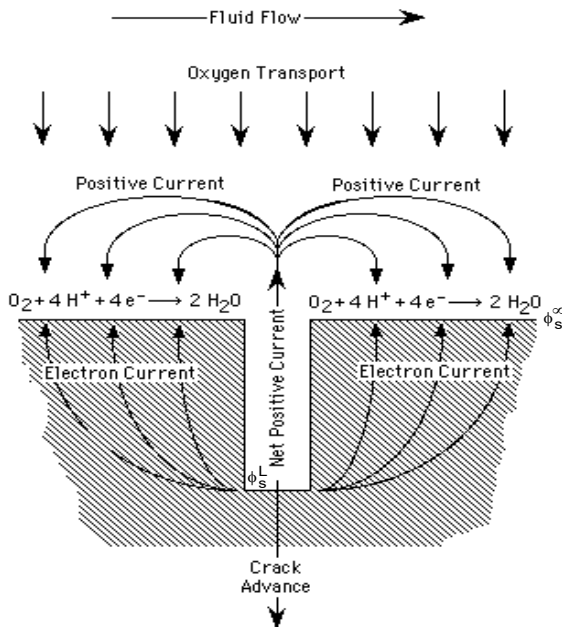
Figure 8: Schematic illustration of the origin of the coupling current in localized corrosion. The arrows indicate the flow of positive current from the pit cavity to the external surface where it annihilates with the electron current flowing from the pit cavity surfaces through the metal to the external surface via the OER.

In this scenario, the HOIs of neighboring pits overlap (Figure 9) and hence the pits compete for the same resources (oxygen reduction) and, in a "survival of the fittest" contest, one pit must die when there are insufficient resources available from the external surfaces to maintain the two active simultaneously. Importantly, this mechanism is expected to become increasingly prevalent as the areal pit density (number per unit area) increases, whereas Death by Old Age is expected to be independent of pit density and to

dominate at low pit densities. Figure 10 and 11 indicate that the density of pits on AlAl 4335 in contact with residue is high, so that "death by Conflict" is the likely mechanism of delayed repassivation and hence of pit death. The third scenario, (3) **Death by Misadventure**, is, where for some unpredictable reason, the pit dies, because of the accidental loss of differential aeration. An example of such a process might be the drying of the external surface, such that no electrolyte phase, no matter how thin exists on the external surface to support pit development. We are currently developing theories and models for these processes with the goal of being able to calculate the delayed repassivation constant, γ, in an *ab initio* manner. This would represent a significant step in corrosion science and would open new vistas for corrosion control. This is, because γ is the single most important parameter in controlling the accumulation of localized corrosion damage on a surface and its manipulation would appear to be an effective means of controlling the accumulation of pitting damage. This control might be exerted by suitable inhibitors that would decrease the exchange current density of the cathodic reaction that occurs on the external surface and hence limits the coupling current.
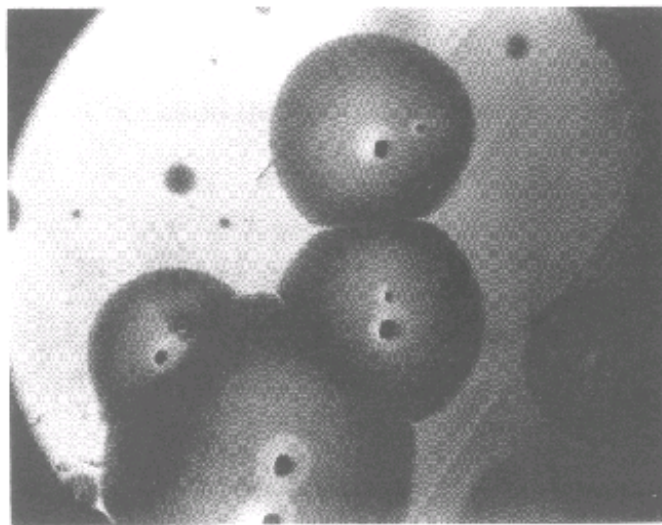
t = 286 s

Figure 9: *In situ* micrographs of nucleating pits on nickel in 0.2 m B(OH)$_3$ + 0.1 m KOH + 2 m KCl at 25 °C under potentiodynamic conditions (1 mV/s from an initial voltage of 0 V$_{sce}$) showing the overlap of the HOIs. [1].
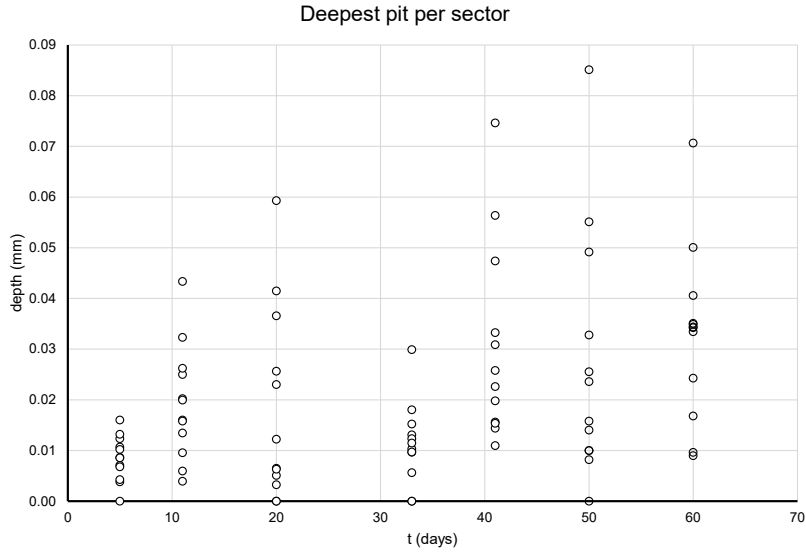
Figure 10: Evolution of the maximum pit depth for flat specimens of AISI 4335 steel in contact with residue at 75 °F and 75 % RH.

In Figure 10, the depths of the deepest pits in ten sectors of equal area are plotted versus the exposure time. In obtaining these data, the area of the exposed flat surface was divided into 12 sectors of equal area and the depths of the deepest pit in each of ten sectors was determined. Clearly, the maximum pit depth for any given area is highly distributed, although a trend toward a constant value can be discerned. This trend is shown more clearly in Figure 11, in which is plotted the average value of the deepest pit versus exposure time.
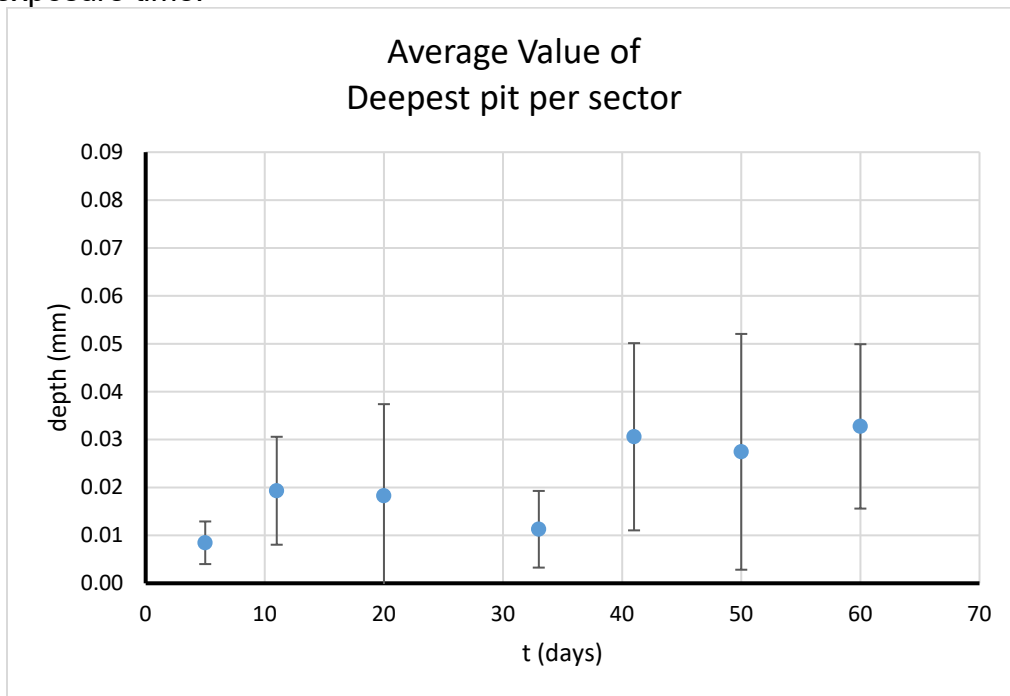
Figure 11: Evolution of the average value of the deepest pit per sector for AISI 4335 steel in contact with residue at 75 °F and 75 % RH.

10

3.2. Damage Function Analysis (DFA) and Deterministic Monte Carlo Simulation (DMCS).

Figure 13 displays a plot of the depth of the deepest flaw (pit or crack) as a function of time. The orange points correspond to pits measured in the laboratory, whereas the blue points correspond to cracks observed on tubes in the field. The reader will note that both sets of data follow a common trend line, even though the times over which each set was obtained are vastly different. This important observation suggests that the evolution of the damage can be described within a common theoretical framework. That framework is Damage Function Analysis (DFA) using a combination of Deterministic Monte Carlo Simulation (DMCS) and Deterministic Extreme Value Statistics (DEVS), as we have described elsewhere [1, 2].

The accumulation of localized corrosion damage in a system is completely defined if we know how many pits or other corrosion events (per cm^2) have depths between x and $x + dx$ for a given observation time, t, at given location on the metal surface. We will denote this quantity as $f_k(x,t)dx$ where $f_k(x,t)$ is the so-called differential damage function (DDF). Here, index k denotes different types of localized defects, such as active and passivated pits, cracks, crevices, and so on. However, in the overwhelming majority of practical cases, especially when the influence of localized corrosion on the quality of the metal surface (e.g. induced roughness due to pitting, if the pitted area is much smaller than the geometric area) can be neglected, it is not important that such detailed information be obtained. Very often, it is sufficient to obtain information about only the deepest corrosion event (pit, crack), because most often the failure of the system occurs when the depth of the deepest corrosion event, L_{max}, increases beyond some critical value, L_{cr}. In that case, for describing corrosion damage, we seek an equation of the following functional form,

$$L_{max} = L_{max}(t, X_i, Y_i)$$
(1)

Here, X_i and Y_i: are internal and external variables, respectively, that determine the damage propagation rate. Examples of internal variable are grain size and orientation, texture, and other micro-structural properties. The external variables include loading and environmental conditions (pH, temperature, [Cl^-], E_{corr}, etc).

However, if even such a function can be obtained, its applicability would be questionable. The problem is that Equation (1) yields a single number for L_{max} for a given t and parameters of the system (i.e., the function yields a "definite" result). However, in the general case, it is impossible to describe the available experimental data by a single number. Thus, the maximum depths of pits measured on different samples taken from the large system usually differ significantly from one to another. Apparently, the best manner of expressing localized corrosion damage and hence in specifying failure would be prediction of the probability of failure, P_f:

$$P_f = P_f(L_{cr}, t, X_i, Y_i, S)$$
(2)

i.e. the probability that at least one corrosion event at any form (pit, stress corrosion crack, fatigue crack) reaches some critical depth, L_{cr}, at a given observation time, t, and given set of environmental conditions. It is also evident that P_f must be a function of the total area of the system, because the larger the area of the system the larger is the number of corrosion events that might have super-critical depths and, accordingly, P_f must increase.

Among the methods of quantitatively estimating this probability can be mentioned Damage Function Analysis (DFA), which contains Deterministic Monte Carlo Statistics (DCMS) and Deterministic Extreme Value Statistics (DEVS) [1, 2]. DFA is based on the solution of differential equations, which are equivalent to a balance equation for the diffusion of a large population of particles in a discontinuous medium and hence relies upon having a sufficiently large population of events that statistical methods are applicable. However, frequently, under real conditions, only a few pits (or cracks), or even only a single pit (or crack), may be alive (propagating) on the corroding metal surface. In this case, the DEVS equations lose their strict physical meaning. The main idea of the Deterministic Monte Carlo Simulation (DMCS) method is to keep track of each stable pit (or crack) that nucleates, propagates, and repassivates (dies) on the metal surface. A great advantage of this method lies in the fact that this approach allows us to take into account the interactions between particular individual pits (cracks) in an explicit manner, as is evident in Death by Conflict. By doing so, it becomes possible to reduce the number of unknown parameters that describe the interaction between individual pits (cracks).

Thus, DMCS allows us to:

- Effectively describe the progression of damage when only several pits, or even a single pit, is alive and propagating; all other pits having repassivated.
- Take into account the interaction between a particular, individual pit (crack) and the remaining (living) pits (cracks) on the surface in an explicit manner.

In the application of the DMCS algorithm at each time step, we have to:

- Determine the location of the newly born active (stable) pits
- Calculate the new dimensions of active pits
- Ascertain if any active pit becomes passive, due to repassivation, or due to overlapping of the HOI with those of other pits
- Check if any pit transition into a crack
- Calculate the new dimension of each crack

It is evident that the applicability of DFA and DMCS requires the existence of deterministic models describing nucleation, propagation, and repassivation of localized corrosion processes. Reviews of these models can be found in Refs 1 and 2. Here, we will describe only the simplest models that have already been used within the framework of the current study. More comprehensive models will be used (and developed) under the subsequent stages of the current work.

Rate of Pit Nucleation

In many practical cases, it is possible to assume that all stable pits on a given surface nucleate during an initial period that is small compared with the observation time, t, or the service life of the system, t_s. For example, for the case of the pitting corrosion of aluminum in tap water, as described by Aziz [22], practically all pits were found to nucleate within the first two weeks, whereas the observation time was typically up to 12 months, giving rise to an "instantaneous" nucleation and growth scenario. A comprehensive deterministic Point Defect Model (PDM) [1-7], which includes instantaneous nucleation as a particular case, will be described in a later paper.

Pit Propagation Rate

The quantitative description of pit (or cavity) growth remains as one of the key challenges in predicting corrosion damage in many practical systems. This follows from the fact that the calculated corrosion damage that is based only on this (growth) stage can be compared with experiment, in many limiting cases. For example, in the case of pitting corrosion, when all pits nucleate "instantaneously", or when the induction time for pit nucleation is much smaller than the observation time, it is possible to ignore the initial stage of pit nucleation when estimating the damage. In addition, if the probability of survival of a corrosion defect is sufficiently high, we must recognize the possibility that a stable corrosion defect (pit or crack) that nucleates immediately after the start of operation and propagates without repassivation may still be active at the end of the observation time. In this case, the growth time alone is all that is required. However, corrosion cavities die for a variety of reasons, as described earlier in this paper, and the deepest pit in the "instantaneous nucleation and growth scenario" corresponds to that which is longest lived, but not that which is necessarily alive at the time of observation. In any case, calculations based only on the growth stage yields the most conservative estimate of the service life, $t_{s,min}$, of the system. We can be sure that, if calculation of the service life is based on growth alone, the real service life, t_s, will, at least, be not less than $t_{s,min}$.

Detailed review of a great number of papers dealing with mathematical modeling of transport phenomenon in localized corrosion and estimation of individual corrosion cavities propagation rates can be found, for example, in Refs. 1, 2, 7-20. It must be mentioned that, in the general case, the solution of the mass transfer problem must be performed both inside and outside corrosion cavities within the framework of the "coupled environment" models [7-20].

It also important to note that, despite the complexity of quantitatively describing pit propagation, it is well-known from experiment that the rates of individual pit (crack) propagation as a function of time under constant environmental conditions can be approximated by a relatively simple function of time. Thus, for the case of pitting corrosion, the power function

$$L = kt^m \tag{3}$$

has been suggested, where k and m are empirical constants [9-11]. Here, L is the characteristic pit size (e.g., pit depth or radius of the pit mouth). Published values of m are very often approximately equal to 1/3, 1/2, 2/3 or 1, but they can also vary over wider ranges [23-28].

However, this dependence of L on t cannot be used directly in mathematical calculations for small times, because of the nonphysical limit, for the pit propagation rate

$$V = \frac{dL}{dt} = kmt^{m-1} \rightarrow \infty \text{ at } t \rightarrow 0 \tag{4}$$

Therefore, instead of Equation (3), the following interpolation equation for pit propagation rate, V, has been suggested [1]

$$V = \frac{V_0}{(1+t/t_0)^p} \tag{5}$$

where V_0 is the initial rate of pit propagation. For small times, as follows from Equation (5), L can be presented as the linear function of t, and for large times, L takes the form of Equation (4). In many cases, the period of time over which the approximation

$$V \approx V_0 = \text{constant} \tag{6}$$

can be comparable with the observation time (or even with the service life of the system). The reason is that corrosion is, generally speaking, a slow process and under real, practical conditions, values of the critical pit depth of the system, x_{cr}, and typical service life, t_s, impose significant restrictions on the values of the initial and average corrosion current densities and, thus, on the potential and concentration drops that might be observed in a corrosion cavity [10].

We will assume that propagation rate of any pit is described by Equation (6), where parameter, V_0, which describes, among other things, that the properties of protective oxide films are statistically distributed. Of course, generally speaking, these properties can change with time. However, we will assume that V_0 does not change with time, for the following reason. This simplification assumes that if one pit speeds up (for example, due to destruction of the protective film), another randomly selected pit might slow down (due to growth of passive film) and both effects compensate one another from the point of view of propagation of a large ensemble of pits.

More precisely, we will assume that parameter, V_0, is distributed normally with a mean value (most probable value) $V_{p,m}$ and with the standard deviation, σ_p. Moreover, because experiments show that, usually, most pits in systems have very small depths, Turnbull et al., suggest that a mean value of zero (by rejecting negative values as being physically unrealistic) can be considered as to be good approximation for a real system [28, 29]. However, it appears evident that pit can be visible if only its rate of propagation is greater

than the general corrosion rate, V_{gc} (that is the pit must "outrun" the loss of metal due to general corrosion). Accordingly, the choice $V_{p,m} = V_{gc}$ is more reasonable. Of course, we will reject values less than V_{gc} as being physically unrealistic.

As was mentioned previously, the interaction between growing pits can inhibit pit propagation, due to the neighboring pits competing for the same resources (cathodic reaction) on the external surface and because one pit will depress the potential experienced by the other (i.e., one pit will "cathodically protect" the other, if sufficiently close). However, our model calculations show that the influence of this effect is practically negligible for the assumed values of parameters, but the execution time of the code is substantially increased when pit interaction is included.

Pit repassivation

Let as consider a pit that survives at time, t (i.e., the pit is still active, because of differential aeration). If this time step is sufficiently small, we can express the probability of repassivation, dP_{rep}, by using only the linear term of the Taylor expansion, i.e.

$$dP_{rep} = \gamma dt \tag{7}$$

where γ is the delayed repassivation ("death") constant. In general, γ, is expected to be a function of the external conditions, including the corrosion potential, temperature, and electrolyte composition. Generally speaking, γ is also expected to be a function of the depth of the pit, x, because the local potential in the solution at the cavity surface depends on the IR potential drop in the cavity, i.e. γ might be a function of both the spatial coordinates and time (pit age). Finally, active pits may no longer be viable if the potential, E, at the pit internal surface is less than the repassivation value, E_{rp}. Accordingly, if the value of E_{rp} is reached at some pit depth, x_{rp}, active pits passivate and cannot penetrate further into the metal. The value of repassivation potential E_{rp}, is a function of the metal potential and surface concentrations at the pit tip. It can be estimated, for example, by using commercially-available software [31, 32].

In general case, we must take into account that if the HOI of two pits overlap, one of them (the one with the smallest HOI) can be declared as "dying" and as being, eventually, "repassivated (dead)". A more correct procedure of describing overlapping of pits is described in [1]. However, our model calculations show that the influence of overlapping on the propagation of pitting corrosion is practically negligible for the assumed (for the current project) values of parameters, and the execution time of the code increases dramatically when this phenomenon is included in the calculation.

Crack Initiation and Propagation

The criteria for the nucleation of a crack from a pit has been given by Kondo [33] and can be formulated in the cases of stress corrosion cracking (SCC) and corrosion fatigue (CF) as:

$K_I > K_{ISCC}$ (for SCC)   or $\Delta K > \Delta K_{th}$ (for CF)   (8)

and

$V_{cr} > V_p$.   (9)

Here, the stress intensity factor for crack nucleation, K_{ISCC} is the minimum Mode I loading stress intensity factor for growth of a crack in Stage I of the crack growth rate vs. stress intensity correlation, ΔK_{th} is a threshold intensity factor, V_{cr} is the growth rate of the just-nucleated crack, and V_p is the growth rate of the just-transitioned pit. The first criterion defines the mechanical condition for crack nucleation, while the second simply says that the nucleated crack must be able to "out-run" the pit to develop as a *bone fide* crack.

In many case, particularly for the high strength steels, such as 3NiCrMoV low pressure steam turbine disc steel, the rate of crack propagation can be described by a simple empirical equation as a function of the applied stress, σ, and the crack depth, L, in the form [24,28-30]:

$$\frac{da}{dt} = C\sigma^p a^q$$ (10)

It was also assumed that parameters p and q are fixed and were determined by fitting Equation (10) to the experimental data, but parameter C was assumed to be normally distributed. However, there is a series of experimental works (see Review 34) where it appears that the rate of crack propagation in some steels is satisfactorily described by an averaged (mean) propagation rates, $V_{cr,m}$, which depends on temperature and the nature of the steel (mainly on the yield strength). Accordingly, at this stage of the investigation, we assume that $p \approx 0$ and $q \approx 0$, but we will assume that the parameter C is normally distributed (but depends on temperature and yield strength).

We would like to emphasize that it is very difficult to explain the transition of a pit into a crack by ignoring the phenomenon of pit repassivation, if the rate of crack propagation is described by the slip/dissolution/repassivation theory. Thus, in accordance with the slip-dissolution model, crack advance is an electrochemical process that is periodical in nature. The protective oxide film at the tip of the crack is ruptured under an increasing strain, due to the imposed, tensile load. Anodic dissolution then proceeds at the crack tip until repassivation occurs. Maximum anodic current (crack propagation) occurs when the crack tip surface is free from the protective oxide film, corresponding to an active cavity tip surface. It is also clear that the average crack propagation rate must be less than the pit propagation rate and it is unclear how the crack can "out-run" a "living" (propagating) pit, to satisfy the second of Condo's criteria, unless the pit is dead. Thus, any dead pit satisfies the last Kondo criterion. Accordingly, to inquire into the dynamics of crack nucleation, it appears to be necessary to ascertain if any of the "dead" (repassivated) pits are sufficiently deep to yield a stress intensity factor that exceeds K_{ISCC} and hence to act as pit nucleation sites. From this brief analysis, we conclude the cracks most likely nucleate at dead pits.

3.3. Crack Initiation and Propagation Due to Cycling

It must be noted that crack initiation and propagation has some particular issues resulting from transient loading, which manifest as a fatigue loading component. Of course, the first Kondo condition:

$$\Delta K > \Delta K_{tr} \tag{11}$$

continues to hold, where ΔK is the Mode 1 stress intensity range and ΔK_{tr} is the critical (or threshold) stress intensity range for fatigue crack growth rate. However, the second condition (crack must overrun the pit) must be redefined. To be specific, let us assume that fatigue crack propagation rate is described by Paris' law:

$$\frac{da}{dN} = C\Delta K^m \tag{12}$$

where C and m are material constants and N is the number of load cycles. Let us denote by, t_{cyc}, the cycle period. In accordance with Paris' law, propagation of the crack over one cycle is $\Delta a = C\Delta K^m$ and it is naturally to declare the value of

$$V_{cyc} = \frac{\Delta a}{t_{cyc}} = \frac{C\Delta K^m}{t_{cyc}} \tag{13}$$

as the crack propagation rate. Thus, the value of V_{cyc} must be used in the second Kondo's conditions for pit to crack transition, as it is in practically all published works (see, for example, [36-38]):

$$V_{cyc} > V_{pit} \tag{14}$$

However, in this case, it is natural to subdivide the cycle period, t_{cyc}, (the period of time between the beginning of the cycling until the beginning of the next (sequential) cycling into two parts:

$$t_{cyc} = t_i + t_p \tag{15}$$

where the impulse time, t_i, is the period of time between the beginning and the end of the cycling stage (when the driving force is $\Delta K > 0$) and the pause time, t_p, (period of time between the end of the force stage until the end of the cycle), when no force occurs ($\Delta K = 0$), during which the crack does not propagate due to the load of the applied force. It must be noted that t_i and t_p are absolutely different in order of magnitude. Thus, t_i is of the order of ms whereas t_p is of the order of minutes (in the case of service) or even years (periodic testing).

It is helpful in this analysis to introduce the physical rate of crack propagation (at impulse period) as

$$V_i = \frac{\Delta a}{t_i} = \frac{C\Delta K^m}{t_i} \qquad (16)$$

and to use the condition:

$$V_i > V_{pit} \qquad (17)$$

instead of traditional Kondo Condition (14). Moreover, due to the condition:

$$t_i << t_{cyc} \qquad (18)$$

we have

$$V_i >> V_c \quad \text{and} \quad V_i >> V_p \qquad (19)$$

i.e. the second Kondo always applies during the impulse period for any reasonable values of the physical parameters. Accordingly, any corrosion pit (regardless of being active or passive) will be overrun (and can be considered as a moving crack) during the impulse period, if the first Kondo condition 11) is satisfied. Thus, by the application of DMCS algorithm, any pit for which Conditions (11) and (19) are satisfied at any time step, Δt, receives the following addition to its depth:

$$\Delta a = C\Delta K^m n \qquad (20)$$

where n is the number of applied cycles in the given time interval $(t, t+\Delta t)$. In our particular case, when we do not know the history of a particular tube, we simply assume that any corrosion cavity (active and passive pits or even cracks) for which Conditions (11) and (19) are satisfied also exhibit an enhanced propagation rate (which will be added to their "rest" propagation rates):

$$V_{cyc} = C\Delta K^m f \qquad (21)$$

where f is the applied firing frequency (15 firings/year in our case).

Extrapolation in Space

In accordance with the general principles of the Deterministic Monte Carlo Simulation (DMCS) method for a given observation time, t, we perform M simulations as described above and, accordingly, receive M values $x_1^*(t), x_2^*(t),..., x_M^*(t)$ for the depth of the deepest cavities. After that, we calculate the average (mean) value of the depth of the deepest cavity as

$$X_{av}(t) = \frac{1}{M}\sum_{m=1}^{M} x_m^*(t) \tag{22}$$

and the standard deviation as

$$\sigma(t) = \sqrt{\frac{1}{M-1}\sum_{m=1}^{M}\left(X_{av}(t) - x_m^*(t)\right)^2} \tag{23}$$

These values describe localized corrosion damage on the model coupons. In order to extrapolate localized damage to the total area of the system we assume that the depths of the deepest pits obey the Type I Weibull distribution [35]. Accordingly, the scale parameter, α, and the center parameter, u, of the distribution for the model sample can be found from the expressions [35]:

$$\alpha = \frac{\sigma\sqrt{6}}{\pi} \tag{24}$$

and

$$u = X_m - \alpha E \tag{25}$$

where $E = 0.57721$ is the Euler constant. After that, the mean value of the deepest flaw on the whole bore hole surface of area S can be found from the relation

$$X_{av,S}(t) = X_{av}(t) + \alpha[E + \ln(S/s)] \tag{26}$$

where s is the area of the sample. The standard deviation in the depth of the deepest pit, σ, does not depend, in this case, on surface area.

Finally, probability of Failure of the whole system, P_f, can be estimated via the relation:

$$P_f = 1 - exp\{-exp[-\left(L_{cr} - u + \alpha ln(S/s)\right)/\alpha]\} \tag{27}$$

where L_{cr} is the critical depth. It is important to note that in general case, L_{cr}, decreases with time due to general corrosion [1], but in this case the correction was judged to be negligible.

Example of Application of DMCS to the Case of Corrosion in Bore Evacuators

Below we show that DMCS can reasonably reconcile the observed experimental data for short term experiments (obtained on coupons) with long term observations (obtained in the field in in bore evacuator regions). All these data were delivered by U.S. Army Combat Capabilities Development Command Armaments Center (DEVCOM AC) in the form of the

depth of the deepest cavity. By performing model calculations, we assume the values of various model parameters that are shown in Table 2.
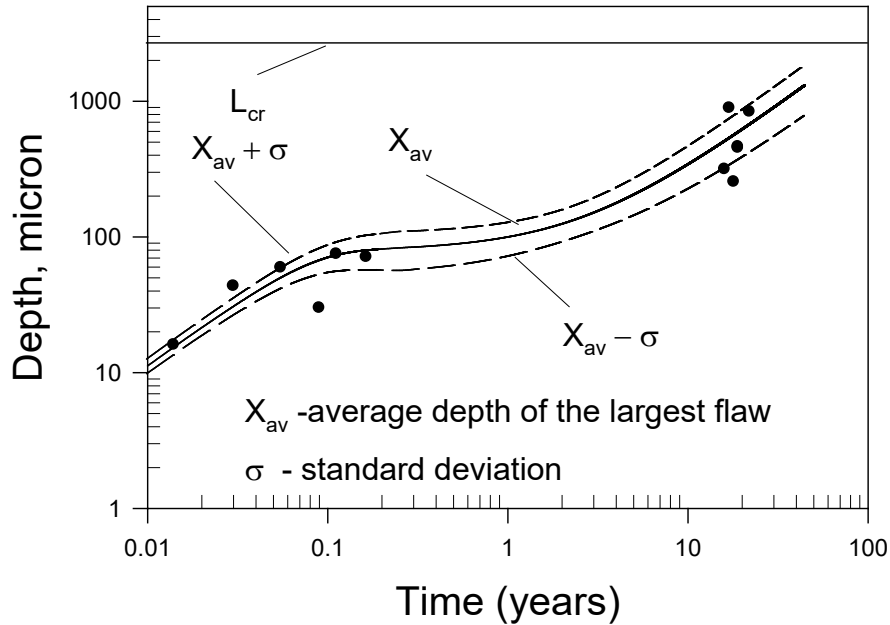

Figure 12: Average depth of the deepest flaw as a function of time. Black circles are experimental data, lines are calculated values. L_{cr} is the maximum allowed penetration into the metal by general corrosion.

Table 2: Parameter values after optimization of DMCS on experimental data.

Parameter	Value
Average area of coupons	92 cm^2
Number of stable pits per coupon (instantaneous nucleation)	330
Area of fielded tubes	76 cm^2
Critical thickness, Lcr	2.6 mm
Repassivation constant, γ	40 y^{-1}
Mean (most probable) pit propagation rate, $V_{p,m}$	6x10^{-10} cm/s
Standard deviation of pit propagation rate, σ_p	2 $V_{p,m}$
Threshold depth, L_{tr}	50 ´µm
Mean (most probable) pit propagation rate, $V_{cr,m}$	2.5x10^{-11} cm/s
Standard deviation of crack propagation rate, σ_p	2 $V_{cr,m}$

The values for the average area of the coupons and the area of the bore holes in the field tubes correspond to the real systems. Threshold depth L_{tr} at which the value of stress intensity factor K_I reaches the value of K_{ISCC} and accordingly cracks at $L > L_{tr}$ can be observed are taken from the experimental data (see Figure 13) that we received from DEVCOM AC. As we can see pits with the depths smaller than approximately 50 µm do not nucleate cracks.
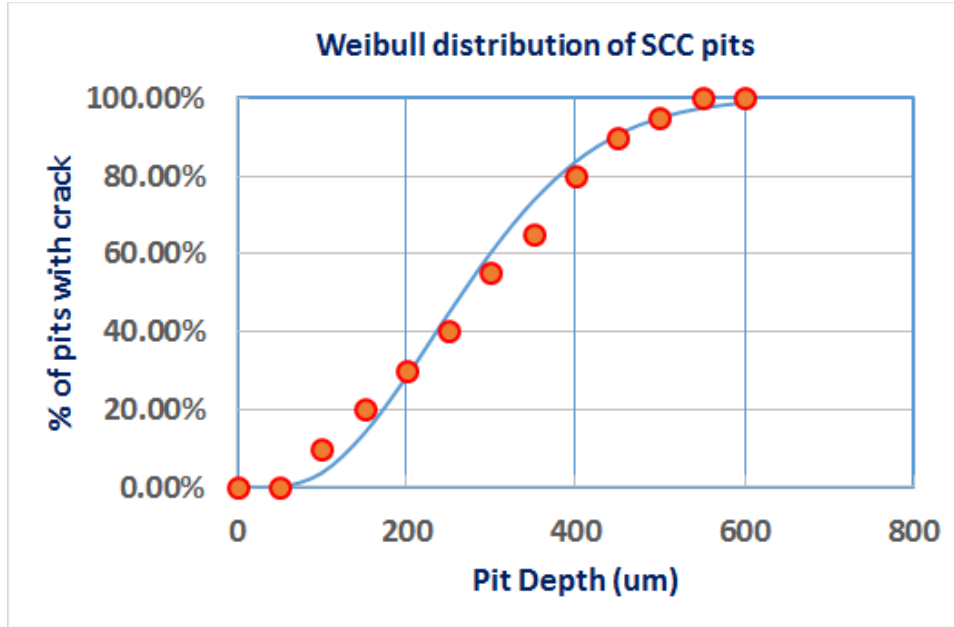
Figure 13: Percentage of pits with crack as a function of pit depths. Circles are experimental data.

Numbers of stable pits per coupon approximately correspond to the data that we obtained from the sponsor. The values of mean propagation rates for pits and cracks and repassivation constant were fitted on experimental data.

Calculation shows that firing (the "corrosion fatigue" effect) practically does not influence the propagation of corrosion damage for the adopted values of parameters. These calculations were performed by using the upper limit for CF propagation rate, which in accordance with the data obtained from the sponsor has the form:

$$\frac{da}{dN} = 8.28 \times 10^{-10} \, \Delta K^{2.73} \text{ in/cyc} \tag{28}$$

where the firing driving force ΔK is shown in Figure 13.
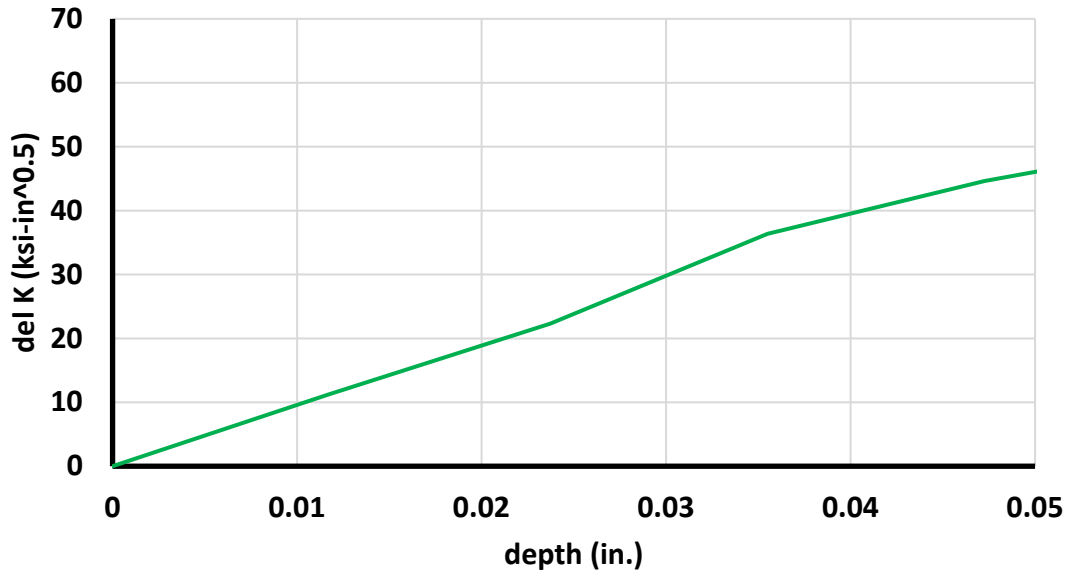
Figure 14: Driving force for crack propagation rate as a function of the crack depth in accordance with the U.S. Army Combat Capabilities Development Command Armaments Center data.

For our model calculations, we approximate these data by the following linear analytical expression: $\Delta K = 1000\, a$, where a is the depth of crack. Here, in accordance with Figure 14, the depth, a, is expressed in inches and the driving force ΔK is given in units of ksi-in$^{1/2}$. A FORTRAN computer code, which reproduces the data shown in Figure 14, was used in the calculation. Generally, the predicted effect of firing is not important, but, under some conditions (increasing of applied stress and/or loading frequency) the loading effect can be significant.

Figure 15: Average depth of the deepest flaw as a function of time for $\gamma = 0, 5, 10, 40, 80, 120$ 1/y.

22

As we can see in Figure 15, the propagation of corrosion damage with time (at sufficiently long periods) is observed. In order to explain this effect, let us consider Figu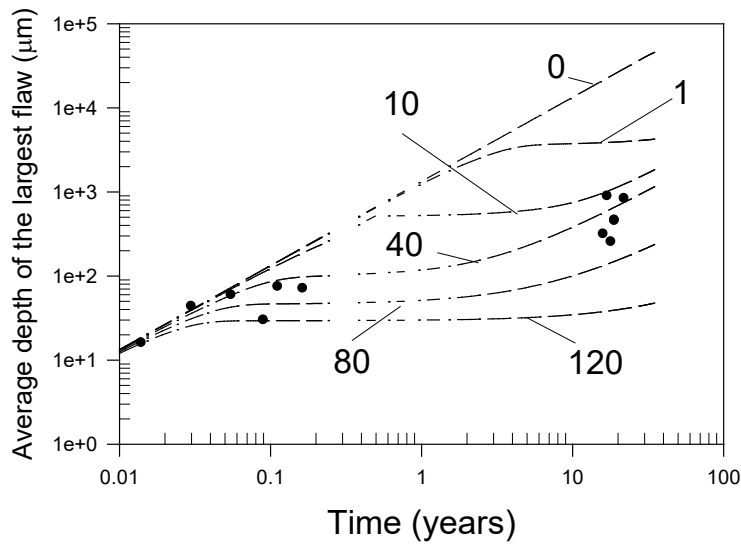re 14, which illustrates the influence of repassivation constant γ on propagation of corrosion damage. This acceleration, for example with time for $\gamma = 40$, is the consequence of the fact that $V_{pit} \gg V_{cr}$. At short period of times only pits determine $X_{max,av}$. However, after a sufficiently long period, practically all pits are dead or have been transformed into cracks. But, because the rate of crack propagation of a newly born crack is very low, they practically do not appear initially to be cracks. Accordingly, we can see a plateau on the graph. However, after a sufficiently long period, we observe the results of crack propagation (plateau transforms into an "up-hill" trajectory). Figure 14 also clearly shows that increasing the repassivation constant might be an effective way of decreasing the accumulation of localized corrosion damage, as has been noted above and previously [1]. Thus, DFA predicts that, if γ is sufficiently large, all pits must be dead after some period and cracks will not be initiated in the system.

Figure 16 and 17, which were calculated using Equation (27), show the influence of critical depth, L_{cr}, and service life on the probability of failure of the system. As we might expect, the probability of failure decreases with increasing L_{cr} and increases with the increasing service life. We find that the tubes examined in this work will be safe if $L_{cr} < 2.7$ mm and the service life is 35 years, because the probability of failure will be less than 1 %. Of course, here we assume that the conditions in the field will not change dramatically with time.
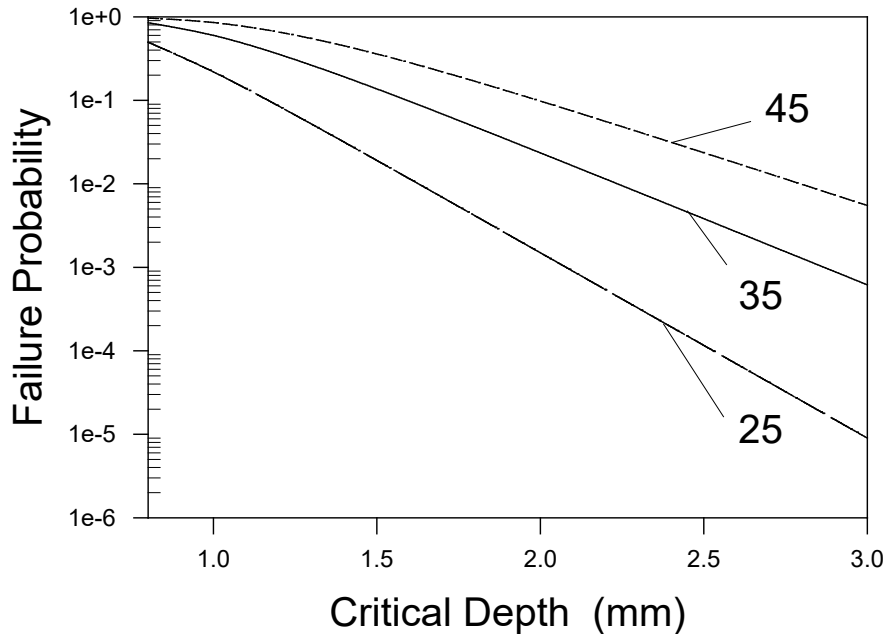

Figure 16: Failure probability as a function of critical depth for service lives of $t = 25$, 35 and 45 years.
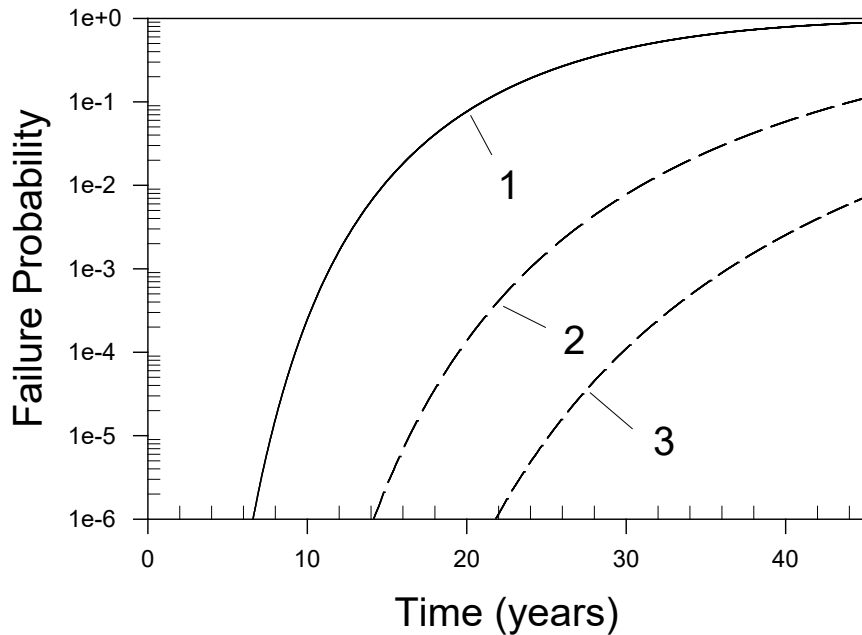
Figure 17: Failure probability as a function of time for critical dimensions of L_{cr} = 1, 2 and 3 mm.

3.4. Importance of Measuring Damage Functions

It must be noted that the direct comparison of the measured damage functions and those predicted by using DMCS cannot be performed, because of the following reason. Each run of the DMCS algorithm yields essentially a different damage function. Of course, we could repeat the calculations many times (for example, 2000 times) and receive a reliable mean (most probable) distribution. Experiments also show that damage functions measured under the same conditions on different coupons can give substantially different results [1]. Thus, the depths of the deepest pits can differ by more than 300 %. However, in the case of experiments, the available time prevented us to obtain statistically-meaningful results. Accordingly, it was expected that great difficulty would be experienced in performing real comparison between averaged damage functions (calculated and measured). These problems have been previously noted in this paper.

However, measurements of damage functions can yield very important information about the order of magnitude of the delayed repassivation constant, pit density, and distribution of pit and crack propagation rates. Thus Figures 18 and 19 display experimental damage functions measured in independent experiments for 5 and 11 days at DEVCOM AC. The experimental data are presented in the form of integral damage functions, $F(x)$, i.e. in the number of pits that have depth less than x. The experiments show that the pit distributions in depth have long tails. It is difficult to describe such data by using a normal distribution in pit growth rate, as is usually done.

One of the simplest possibilities of describing these data is in terms of a Pareto distribution, which is often used to model the distribution of incomes. This distribution

states that the proportion of the population whose income exceeds any positive number $x > x_m$ is $\left(\dfrac{x_m}{x}\right)^{\alpha}$, where x_m is a minimum income and α is the Pareto index. Since a proportion must be between 0 and 1, inclusively, the index α must be positive, but for the total income of the whole population to be finite, α must also be greater than 1. The larger the Pareto index, the smaller the proportion of very high-income people.
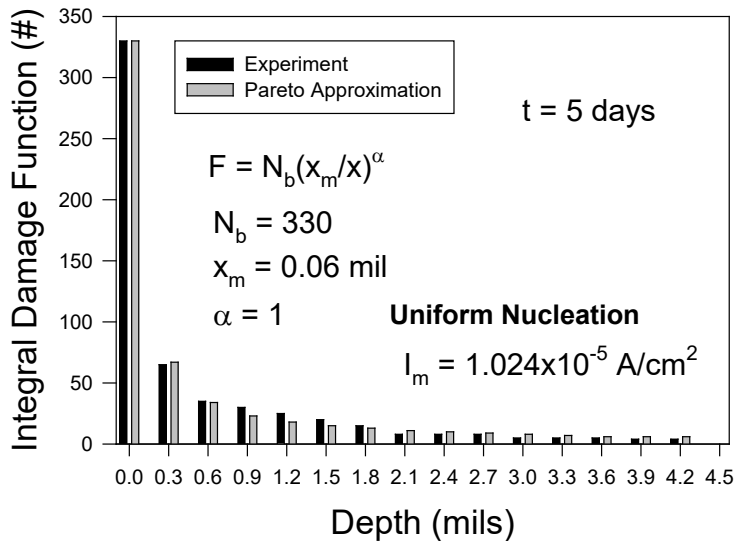

Figure 18: Experimental and fitted Pareto integral damage functions observation time 5 days.
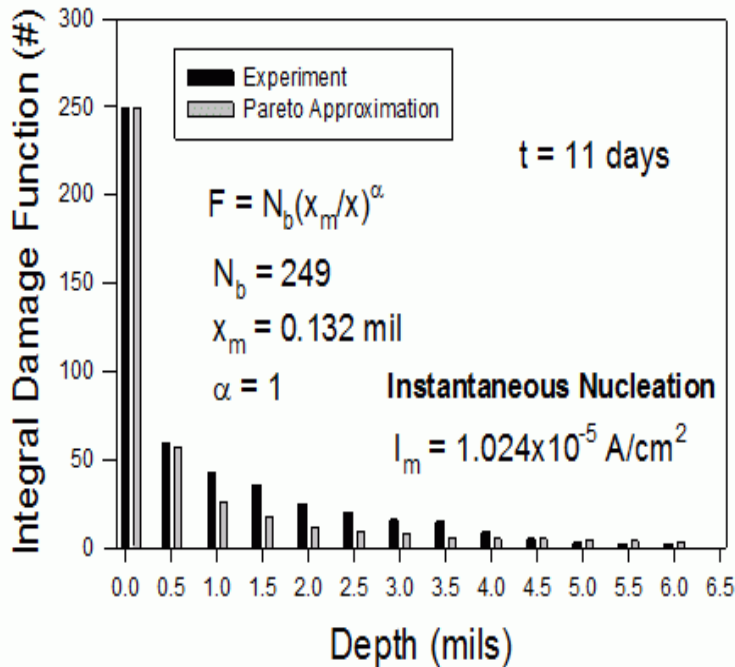

Figure 19: Experimental and fitted Pareto integral damage functions observation time 11 days.

In accordance with the Pareto distribution, the integral damage function for pits has the form:

$$F(x,t) = N_b(t)\left(\frac{x_m}{x}\right)^{\alpha} \tag{29}$$

where $N_b(t)$ is the number of stable pits that nucleate in the time interval between 0 and t, and x_m is the minimum possible pit depth relative to the initial position of the surface (general corrosion damage). If experiments were performed at relatively short observation times (when we can neglect the pit repassivation phenomenon and changes in pit propagation rate due to diffusion limitations), the corresponding distribution of the pit relative propagation rates has the form:

$$\left(\frac{V_m}{V}\right)^{\alpha} \tag{30}$$

and this distribution can be used in Deterministic Monte Carlo simulation of the corrosion damage. Here, V_m is the minimum rate of pit propagation, which can be considered as a general corrosion rate, with the corresponding corrosion current density, I_m. It is important to note that, in the pitting case, there is no restriction $\alpha > 1$, because the rate of pit propagation is limited by the physical limitation $V \leq V_{lim}$. The value of V_{lim} can be obtained from deterministic models, for example, Coupled Environmental Pitting Model (CEPM) [1].

In Figure 18 parameter x_m (general corrosion damage) is simply increased by the factor (11 day/5 day) = 2.2 in comparison with the damage functions shown in Figure 16 with x_m = 0.06 mil and with the parameter α being kept constant. The fact that, after increasing of parameter x_m by 11/5, without changing the value of the parameter α, yields such good agreement between the measured and calculated integral damage functions clearly shows that Pareto distribution can be used instead of the normal distribution for estimating pit propagation rates.

3.5. Possible Crack Arrest

The stress distributions strongly suggest that crack arrest for mechanical reasons will be an important factor in determining the accumulation of damage at long exposure times. Thus, the residual hoop stress is predicted to decrease rapidly with distance into the steel away from the hole surface. Furthermore, as demonstrated by the data presented in Figure 3, the residual stresses are expected to further relax as the damage as the crack propagates and especially so if multiple cracks propagate, in addition to the relaxation of the residual stress. Therefore, the effective stress intensity

$$K_I = A\sigma\sqrt{\pi a} \tag{31}$$

where σ is the effective stress, A is a geometry-specified constant, and *a* is the crack length, is expected to decrease with time, because the decrease in σ is expected to outweigh the increase in crack length, *a*. When $K_I = K_{ISCC}$, the crack will arrest. We see no scenario where $K_I \rightarrow K_{IC}$ and catastrophic failure might occur, except unless the transient operational stress lasting a few milliseconds over each loading were to overwhelm the declining residual stress.

These issues are not addressed in depth in the present report, but will be analyzed in later paper. However, we have derived an algorithm for addressing crack arrest, comprising the following steps:

1. Fit the compliance equation

$$K_I = K_I^0 + a(L - L^0) + b(L - L^0)^2 + \cdots \qquad (32)$$

   to the K_I vs crack length data (Figure 3), where K_I^0 is the stress intensity at the initial crack length, L^0, and *a*, *b*, ... are regression coefficients.
2. Fit crack growth rate vs K_I - K_{ISCC} data from Figure 4, to a Paris-type equation

$$\frac{dL}{dt} = B(K_I - K_{ISCC})^n \qquad (32)$$

   where *B* and *n* are regression coefficients.
3. Using these equations, calculate the crack growth rate for the initial K_I and for $L = L^0$.
4. Increment the time by Δt and calculate a new crack length as *L(j)* =*L(j-1) + (dL/dt)*Δt.
5. For the new crack length, *L(j)*, use the compliance expression and the residual stress distribution to calculate a new effective stress intensity factor for the crack.
6. Repeat Steps 2 and 3 and for each j compare K_I with K_{ISCC}. When K_I becomes equal to or less than K_{ISCC} the calculation ceases as the Kondo criterion is no longer satisfied and the crack has died (arrested). This procedure yields the critical crack length.
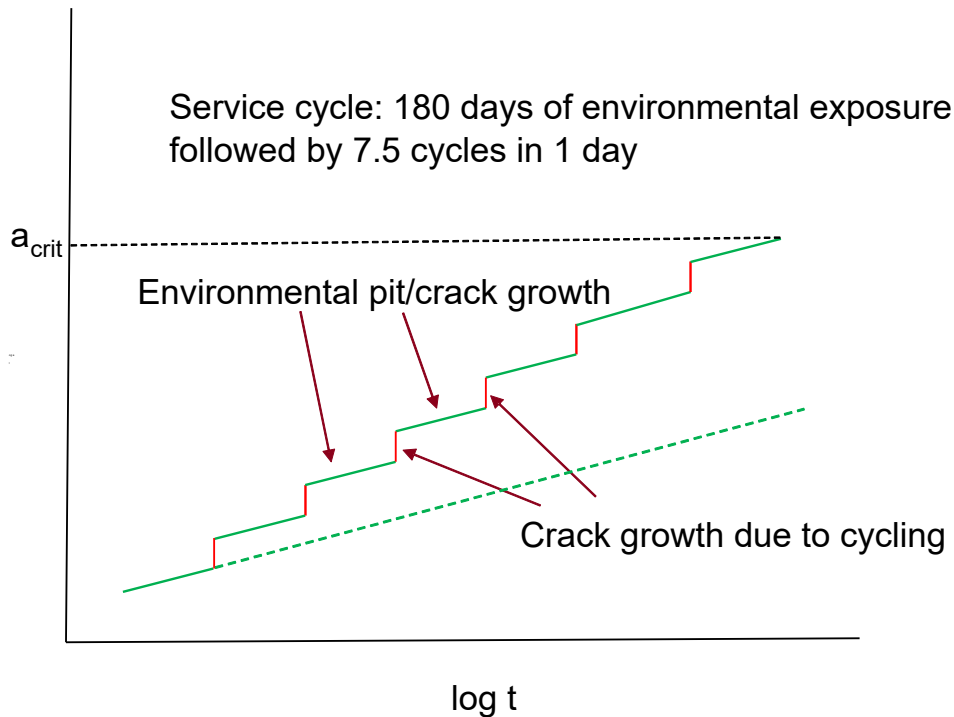
Figure 20: Notional schematic of the likely impact of cycling on the flaw depth.

Finally, Figure 20 depicts schematically the contribution that cycling the tube might make to the accumulated damage. Because the time over which the stress is elevated during firing is very short (approx. 10 ms), the jumps in the crack length are estimated to be of the order of 10^{-7} (10^{-5} mm/s x 10^{-2} s) mm for each event. Thus, if the tube were cycled 100 times, the crack length might increase by 10^{-5} mm, which appears to be negligible, but this should be regarded as being little more than a "guesstimate" and must be subjected to a more thorough analysis.

3.6. Conservativeness of the Predictions

In our opinion, the present calculations are highly conservative for the following reasons:

- We assume the sharp crack expression for the stress intensity of a blunt (e.g., hemispherical) pit. Accordingly, the stress intensity factor for the pit is grossly over-estimated, resulting in a grossly underestimated crack initiation time and critical depth.
- The present calculation does not include the residual stress distribution or stress relaxation, because of the propagating cracks, so that the stress intensity at crack nucleation and for a propagating crack are significantly over-estimated.
- The present calculations do not incorporate an experimentally-derived value for the delayed repassivation constant (DRC), γ. The DRC is judged by the authors to be the single most important parameter in DFA in controlling the progression of damage, as demonstrated by parametric studies reported in this report.

On the other hand, the crack growth rates for AISI 4335 steel in contact with residue, is unexpectedly high (10^{-6} mm/s to 10^{-5} mm/s), which is several orders in magnitude greater than CGR in the closely-related ASTM A470/471turbine disk/rotor steel [34]. Clearly, these measurements must be repeated and judgment of the importance of this factor is deferred until that has been done. On balance, we have great confidence in the conservativeness of the predictions presented in this report and that the risk of catastrophic failure is as low as indicated.

4.   **Summary and Conclusions.**

As a result of an analysis of the observed pitting and cracking in the vent holes in AISI 4335 steel tubes, we summarize our findings as follows:

- Pitting and subsequent cracking may be attributed to localized corrosion beneath a layer of residue on the bore hole surface.
- The residue contains a high concentration of chloride ion, which is well-known to be a powerful agent in affecting passivity breakdown and pitting on high strength steels like AISI 4335.
- The measured corrosion potential at three locations on an AISI 4335 sample in contact with a slurry of residue under prototypical field conditions was found to be -0.255 ± 0.021 V_{she}. The electrochemical conditions are judged to be conducive to passivity breakdown and hence pitting corrosion.
- The stress state of the region, as determined by finite element analysis, is conducive to the nucleation of cracks from pits.
- Pits with depths greater than approximately 50 μm nucleate cracks.
- The impact of stress transients during firing of the accumulation of the observed damage (crack length) is judged to be negligible.
- Damage Function Analysis (DFA) using a Pareto distribution for crack growth rate successfully accounts for the evolution of localized corrosion damage and provides an effective means of extrapolating damage to future times, provided the environmental conditions remain constant.
- The threshold life-time can be confidently extended to 28 years.
- Although much remains to be done to refine the models upon which these predictions are based we have a high level of confidence in extending the service limit to the threshold and objective dates, assuming a maximum allowable flaw of 2.69 mm in a population of 226.

4. **Acknowledgments**

5. References

1. D. D Macdonald and G. R. Engelhardt, Predictive Modeling of Corrosion. In: Richardson J A, et al. (eds.) *Shrier's Corrosion*, **2**, 1630-1679 (2010).
2. D. D. Macdonald and G. R. Engelhardt, "A Brief Review of Determinism in the Prediction of Localized Corrosion Damage", *Z. Phys. Chem*., **226**, 1–18 (2012).
3. D. D. Macdonald. "On the Existence of our Metals-Based Civilization: I. Phase Space Analysis," *J. Electrochem. Soc.*, **153**(7), B213 (2006).
4. D. D. Macdonald, "Passivity: The Key to Our Metals-Based Civilization", *Pure Appl. Chem*., **71**, 951-986 (1999).
5. D. D. Macdonald, "The Passive State in Our Reactive Metals-Based Civilization", *Arab J. Sci. Eng*, *37*, 1143–1185 (2012).
6. G. R. Engelhardt, D. D. Macdonald, *Corrosion*, **54**, 469 (1998).
7. D. D. Macdonald, Mirna Urquidi-Macdonald. "A coupled environment model for stress corrosion cracking in sensitized type 304 stainless steel in LWR environments" *Corros. Sci.*, **32**(1), 51-81 (1991.
8. P-C. Lu, D. D. Macdonald and M. Urquidi-Macdonald. "The Coupled Environmental Fracture Model - A Deterministic Method for Calculating Crack Growth Rates". Corrosion/94, NACE Annual Conference and Corrosion Show. Paper #246. pp. 1-22 (February 28-March 4, 1994). NACE International, Houston, TX.
9. G. R. Engelhardt, M. Urquidi-Macdonald M., D. D. Macdonald, *Corros. Sci.*, **39**, 419 (1997).
10. G. R. Engelhardt and D. D. Macdonald. "Estimation of Corrosion Cavity Growth Rate for Predicting System Service Life", *Corros. Sci.*, 46(5), 1159-1187 (2004).
11. G. R. Engelhardt, D. D. Macdonald, M. Urquidi-Macdonald, *Corros. Sci.*, **41**, 2267 (1999).
12. D. D. Macdonald and M. Vankeerberghen. "Predicting Crack Growth Rate vs. Temperature-Behaviour of Type 304 Stainless Steel in Dilute Sulfuric Acid Solutions", *Corros. Sci*., **44**, 1425-1441 (2002).
13. D. D. Macdonald and M. Vankeerberghen. "Calculating the Temperature-Maximum and the Lower Potential Limit for the Crack Growth Rate in Type 304 SS Using the CEFM", CORROSION 2003 (NACE), Paper No.03520 (2003).
14. M. P. Manahan, D. D. Macdonald, and A. J. Peterson, Jr. "Determination of the Fate of the Current in the Stress-Corrosion Cracking of Sensitized Type 304SS in High Temperature Aqueous Systems". *Corros. Sci*., **37**(1), 189-208 (1995).
15. D. D. Macdonald. "On the Modeling of Stress Corrosion Cracking in Iron and Nickel Base Alloys in High Temperature Aqueous Environments". *Corros. Sci*., **38**(6), 1003-1010 (1996).
16. -K. Lee, D. Kramer, and D. D. Macdonald, "On the shape of stress corrosion cracks in sensitized Type 304 SS in Boiling Water Reactor primary coolant piping at 288° C", *J. Nucl. Mat.*, **454**, 359 - 372 (2014).
17. S.-K. Lee, P.-C. Lv, and D. D. Macdonald, "Customization of the CEFM for Predicting Stress Corrosion Cracking in Lightly Sensitized Al-Mg Alloys in Marine Applications", *J. Solid State Electrochem*., **17**, 2319 – 2332 (2013).

18. K. Williams, R. Bayles, and D. D. Macdonald, "Observation of the Coupling Current During Stress Corrosion Cracking of Aluminum Alloy 5083", *J. Electrochem. Soc.*, submitted (2015).

19. J-B. Shi, J. Wang, and D. D. Macdonald, "Prediction of primary water stress corrosion crack growth rates in Alloy 600 using artificial neural networks", *Corros. Sci.*, **92**, 217 – 227 (2015).

20. W. Y. Maeng, Digby D. Macdonald. "The effect of acetic acid on the stress corrosion cracking of 3.5NiCrMoV turbine steels in high temperature water". *Corros. Sci.*, **50**(8), 2239-2250 (2008).

21. S. Sharifi-Asl, M. L. Taylor, Z. Lu, G. R. Engelhardt, B. Kursten and D. D. Macdonald, "Modeling of the Electrochemical Impedance Spectroscopic Behavior of Passive Iron Using a Genetic Algorithm Approach", Electrochim. Acta, 102, 161-173 (2013).

22. P. M. Aziz, *Corrosion*, **12**, 35 (1956).

23. S. M. Sharland, *Corr. Sci.*, **33**, 183 (1992).

24. A. Turnbull, *Br. Corros. J.,* **28**, 297 (1993).

25. S. Papavinosan, W. Revie; W. Friesen, *Corrosion Reviews*, **24**, 173 (2006).

26. L. I. Freiman, In Progress in Science and Technology. Corrosion and Corrosion Protection VINITI, 1985; Vol. 11, pp 3–71 [in Russian].

27. Z. Szklarska-Smialowska, Pitting Corrosion of Metals; National Association of Corrosion Engineers: Houston, TX, 1986.

28. A. Turnbull, L. N. McCartney and S, Zhou, *Corros. Sci.*, **48**, 2085 (2006).

29. A. Turnbull, D. A. Horner, B. J. Connolly. McCartney, S. Zhou, *Eng. Fract. Mech.*, **76**, 633 (2009).

30. D. A. Horner, B. J. Connolly, S. Zhou, and A. Turnbull, *Corros. Sci.*, **53** (2011) 3466.

31. A. Anderko, Modeling of Aqueous Corrosion, In: Richardson J A, et al. (eds.) *Shrier's Corrosion*, **2**, 1585-1629 (2010).

32. www.olisytems.com.

33. Y. Kondo, *Corrosion*, **45**, 7 (1989.

34. T. H. McCloskey, R. B. Dooley and W. P. McNaughton, "Turbine Steam Path Damage: Theory and Practice, V. 2, EPRI, Palo Alto, CA, 1999.

35. P. J. Laycock and R. A. Cottis, P.A., *J. Electrochem. Soc.*, **137**, 64 (1990).

36. G.S. Chen, K.-C. Wan, M.Gao, R.P. Wei, T.N. Flournoy, *Material Science and Engineering*, **A219**, 126 (1996).

37. D. G Harlow, R.P. Wei, *Fatigue Fract Engng Mater Struct,* **22**, 427 (1999).

38. D. G Harlow, R.P. Wei, *Fatigue Fract Engng Mater Struct*, **24**, 523 (2001).